Probing the Higgs boson trilinear self-coupling through Higgs boson + jet production

Jun Gao,[1,2,*] Xiao-Min Shen,[1,3,†] Guoxing Wang,[4,5,6,‡] Li Lin Yang,[4,§] and Bin Zhou[1,‖]

[1]*INPAC, Shanghai Key Laboratory for Particle Physics and Cosmology, School of Physics and Astronomy, Shanghai Jiao Tong University, Shanghai 200240, China*
[2]*Key Laboratory for Particle Astrophysics and Cosmology, Shanghai 200240, China*
[3]*Deutsches Elektronen-Synchrotron DESY, Notkestr. 85, 22607 Hamburg, Germany*
[4]*Zhejiang Institute of Modern Physics, School of Physics, Zhejiang University, No. 866 Yuhangtang Road, Hangzhou 310058, China*
[5]*Institute for Theoretical Physics Amsterdam and Delta Institute for Theoretical Physics, University of Amsterdam, Science Park 904, 1098 XH Amsterdam, Netherlands*
[6]*Nikhef, Theory Group, Science Park 105, 1098 XG, Amsterdam, Netherlands*

(Received 21 February 2023; accepted 25 May 2023; published 14 June 2023)

We present the calculation of the next-to-leading-order corrections for Higgs boson + jet production at the Large Hadron Collider, that arise from the Higgs trilinear self-coupling (λ_{HHH}). We use the method of large top-quark mass expansion to tackle the challenging two-loop virtual amplitude and apply the Padé approximation to extend the region of convergence of this expansion. We find that the λ_{HHH}-related corrections amount to 0.66% for the total cross section. For the invariant mass distribution and Higgs boson transverse momentum distribution, the corrections are mostly in the range 0.5%–0.7%. Our results can be used to set extra constraints on λ_{HHH} from the experimental data.

DOI: 10.1103/PhysRevD.107.115017

I. INTRODUCTION

After the discovery of the Higgs boson [1,2], accurately measuring its properties including various couplings has become one of the top priorities of the LHC. The Higgs boson is related to the spontaneous breaking of the electroweak symmetry and is responsible for the masses of all elementary particles. Also, the Higgs boson may provide the leading portal to possible hidden sectors beyond the Standard Model (SM). In particular, the Higgs trilinear self-coupling (λ_{HHH}) is the key parameter in the Higgs potential. The precise determination of its value will give us a better chance to understand the electroweak symmetry breaking mechanism as well as possible new physics (NP) beyond the SM.

The λ_{HHH} coupling can be measured directly via the double-Higgs boson production. The very recent observed constraints from direct measurements are $-0.6 < \kappa_\lambda = \lambda_{HHH}/\lambda_{HHH}^{\mathrm{SM}} < 6.6$ at 95% confidence level (CL) [3], where $\lambda_{HHH}^{\mathrm{SM}}$ is the Higgs trilinear self-coupling in the SM. However, the double-Higgs production alone is not enough to get precise constraints. On the one hand, because of the accidental cancellation between the triangle- and box-type Feynman diagrams at the leading order (LO) in the gluon fusion channel, the total cross section of double-Higgs production is heavily suppressed [4,5]. On the other hand, when using the double-Higgs production to set the constraints, we need strong assumptions on the Higgs coupling modifiers to other SM particles.

Apart from the double-Higgs production, λ_{HHH} can also appear in the loop corrections to single-Higgs production processes. The observed constraints on λ_{HHH} using the combined single- and double- Higgs production are $-0.4 < \kappa_\lambda < 6.3$ at 95% CL [3], which is better than the constraints from double-Higgs production alone. More importantly, using the single-Higgs production allows us to relax the assumptions on the coupling modifiers to other SM particles, e.g., the coupling modifier between the Higgs boson and the top quark [3]. To investigate this kind of loop effects, the so-called C parameters are introduced in the literature [6,7], where different single-Higgs production channels, including vector-boson fusion (VBF), VH, $t\bar{t}H$, and tHj production processes, are analyzed. Reference [7] has found that the differential distributions of the

*jung49@sjtu.edu.cn
†xmshen137@sjtu.edu.cn
‡wangguoxing2015@pku.edu.cn
§yanglilin@zju.edu.cn
‖zb0429@sjtu.edu.cn

single-Higgs production processes can provide extra sensitivity to determine λ_{HHH}. However, the impacts of differential distributions in the $gg \to H + j$ process have not been considered in Ref. [7] because of the highly nontrivial two-loop Feynman integrals.

Recently, two-loop amplitudes for $pp \to H + j$ involving internal electroweak bosons and light quarks were investigated in Refs. [8–11]. There are no contributions from λ_{HHH} included in these works. To include the effect of λ_{HHH}, we need to consider the contribution from a class of two-loop diagrams with internal Higgs propagators and a massive top-quark loop. The calculation of these diagrams is quite challenging, due to the appearance of two-loop Feynman integrals with two different masses m_t and m_H and two Mandelstam variables $\hat{s}$ and $\hat{t}$. These integrals are still unknown analytically so far. In this case, various approximations can be used to get reliable predictions in certain kinematic regions. In particular, the large top-quark mass approximation has proven to be quite reliable for QCD corrections for $H + j$ production [12,13] and double-Higgs production below the $2m_t$ threshold [14,15]. For the two-loop amplitudes of $H \to ggg$ and $H \to q\bar{q}g$ with a λ_{HHH} coupling, the analytic expressions in the large top-quark mass expansion up to $\mathcal{O}[1/(m_t^2)^3]$ are given in Ref. [16] and are then used to study the effect of κ_λ on the Higgs boson transverse momentum (p_T) distribution [16,17].

In this work, we focus on the calculation of the λ_{HHH}-related next-to-leading order (NLO) corrections to $pp \to H + j$ at the LHC and extract the C parameter for the total cross section as well as differential cross sections. We use the method of large top-quark mass expansion to tackle the challenging multiscale two-loop Feynman integrals. We perform the expansion to much higher orders than in Ref. [16]. Also, to extend the range of validity of the large top-quark mass expansion, we adopt the Padé approximation [18–22]. This enables us to extend our predictions to higher energy regions, which are more sensitive to NP beyond the SM.

This paper is organized as follows. In Sec. II, we briefly introduce our notations and present the λ_{HHH}-related NLO corrections to $pp \to H + j$ at the LHC. In Sec. III, we show our numerical results and give the C parameter at the levels of the total cross section and the differential cross sections. The conclusion comes in Sec. IV. We leave the lengthy expressions of the form factors for Appendix.

II. METHODS

We need to consider four partonic processes, $g_a(p_1) + g_b(p_2) \to g_c(p_3) + H(p_4)$, $q_a(p_1) + \bar{q}_b(p_2) \to g_c(p_3) + H(p_4)$, $q_a(p_1) + g_b(p_2) \to q_c(p_3) + H(p_4)$, and $\bar{q}_a(p_1) + g_b(p_2) \to \bar{q}_c(p_3) + H(p_4)$, where a, b, and c are color indices; $q(\bar{q})$ only refer to light (anti) quarks; and p_i are the external momenta with $p_1^2 = p_2^2 = p_3^2 = 0$ and $p_4^2 = m_H^2$. In our calculation, we neglect the masses of all light fermions except that of the top quark. Hence, we do not consider the diagrams involving the Yukawa couplings between the Higgs boson and the light fermions. Take the gg channel as an example. At the LO, we only consider the diagrams including a top-quark loop, as shown in the upper plots of Fig. 1. Here, one can also include the light-quark loops, e.g., the bottom- and charm-quark loops. However, their contributions to C_1 are suppressed by the Yukawa couplings of the light quarks, i.e., m_q/m_t, with respect to the top-quark contribution, which can be seen from the definition of C_1 in the following. We therefore do not consider these contributions for simplicity. At the NLO (two-loop) level, we select the diagrams with both a top-quark loop and a λ_{HHH} vertex. Note that the diagrams with a light-quark loop and a λ_{HHH} vertex are always suppressed by $(m_q/m_t)^2$ and negligible with respect to the top-quark contribution. With these considerations, there are 21 two-loop Feynman diagrams in the gluon fusion channel, and two of them are shown in the lower plots of Fig. 1. Note that these two-loop diagrams are IR finite and we do not need to consider real emissions.

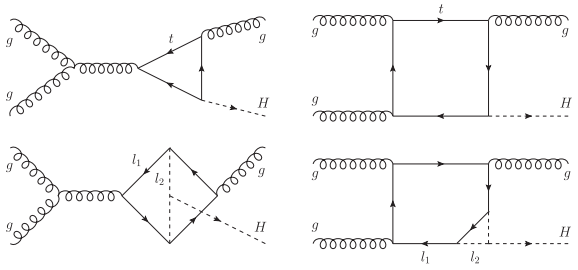

FIG. 1. Typical one-loop (upper) and two-loop (lower) Feynman diagrams for the gluon fusion channel. Dashed lines represent Higgs bosons; solid lines are top quarks; curly lines are gluons. l_1 and l_2 are the loop momenta.

Before describing the calculation procedure, we first review the definition of the C parameter mentioned in the Introduction. Following Ref. [6], we consider a beyond-the-SM scenario where the only modification is $\lambda_{HHH}^{\mathrm{SM}}$, which can be parametrized by a single parameter κ_λ. Therefore, the trilinear Higgs coupling term in the Higgs potential after electroweak-symmetry breaking can be written as $\kappa_\lambda \lambda_{HHH}^{\mathrm{SM}} v H^3$, where v is the vacuum expectation value and H is the physical Higgs field. In the presence of the modified trilinear coupling, a generic NLO observable Σ_{NLO} (e.g., total or differential cross sections) for single Higgs production can be written as

$$\Sigma_{\mathrm{NLO}} = Z_H \Sigma_{\mathrm{LO}} (1 + \kappa_\lambda C_1), \tag{1}$$

where Z_H is the Higgs field renormalization constant, Σ_{LO} is the LO observable which is not modified with respect to the SM, and C_1 is the process- and kinematic-dependent component. Note that the contribution coming from Z_H is universal and common to all single-Higgs production

processes, whose effect can be considered by introducing a C_2 parameter as in Ref. [6]. In this paper, we focus on the process-dependent C_1 parameter. In the limit $\kappa_\lambda \to 1$, $Z_H = 1 + \delta Z_H$, and $\Sigma_{\rm NLO}$ goes to its SM value

$$\Sigma_{\rm NLO}^{\rm SM} = \Sigma_{\rm LO}(1 + C_1 + \delta Z_H), \tag{2}$$

where δZ_H is given by

$$\delta Z_H = -\frac{9}{16\sqrt{2}\pi^2}\left(\frac{2\pi}{3\sqrt{3}} - 1\right) G_F m_H^2, \tag{3}$$

with G_F being the Fermi constant. Therefore, C_1 can be extracted as

$$\begin{aligned} C_1 &= \frac{\Sigma_{\rm NLO}^{\rm SM} - \Sigma_{\rm LO} - \delta Z_H \Sigma_{\rm LO}}{\Sigma_{\rm LO}} \\ &= \frac{\sum_{i,j}\int dx_1 dx_2 f_i(x_1) f_j(x_2) 2\Re(\mathcal{M}^{(0)*}\delta\mathcal{M}^{(1)}_{\rm bare}) d\Phi_2}{\sum_{i,j}\int dx_1 dx_2 f_i(x_1) f_j(x_2) |\mathcal{M}^{(0)}|^2 d\Phi_2}, \end{aligned} \tag{4}$$

where the sum goes over all possible partonic initial states i, j; $f_j(x)$ is the parton distribution function of a parton j with a fraction x of the initial proton momentum; $d\Phi_2$ is the two-body phase-space measure; $\mathcal{M}^{(0)}$ is the one-loop amplitude; and $\delta\mathcal{M}^{(1)}_{\rm bare}$ is the two-loop amplitude without the Higgs field renormalization.

We now turn to the calculation of $\mathcal{M}^{(0)}$ and $\delta\mathcal{M}^{(1)}_{\rm bare}$. The amplitudes for the gg and $q\bar{q}$ channels are given by

$$\begin{aligned} \mathcal{M}^{gg}_{abc} &= \sqrt[4]{2}\sqrt{G_F}\sqrt{4\pi\alpha_s}\mathcal{M}^{\mu\nu\rho}_{abc}\epsilon_\mu(p_1)\epsilon_\nu(p_2)\epsilon^*_\rho(p_3), \\ \mathcal{M}^{q\bar{q}}_{abc} &= \sqrt[4]{2}\sqrt{G_F}\sqrt{4\pi\alpha_s}\mathcal{M}^{\rho}_{abc}\epsilon^*_\rho(p_3), \end{aligned} \tag{5}$$

where α_s is the strong coupling constant. Note that the amplitudes $\mathcal{M}^{qg}_{abc}$ for the qg channel and $\mathcal{M}^{\bar{q}g}_{abc}$ for the $\bar{q}g$ channel can be obtained by applying the crossing symmetry to $\mathcal{M}^{q\bar{q}}_{abc}$. $\mathcal{M}^{\mu\nu\rho}_{abc}$ and $\mathcal{M}^{\rho}_{abc}$ can be written as linear combinations of independent tensor structures, respectively,

$$\mathcal{M}^{\mu\nu\rho}_{abc} = f_{abc}\sum_{i=1}^{4}\mathcal{T}^{\mu\nu\rho}_{gg,i}A_{gg,i}(\hat{s},\hat{t},m_H,m_t), \tag{6}$$

$$\mathcal{M}^{\rho}_{abc} = it^c_{ab}\sum_{i=1}^{2}\mathcal{T}^{\rho}_{q\bar{q},i}A_{q\bar{q},i}(\hat{s},\hat{t},m_H,m_t), \tag{7}$$

where the Mandelstam variables are defined as

$$\hat{s} = (p_1+p_2)^2, \qquad \hat{t} = (p_1-p_3)^2, \qquad \hat{u} = (p_2-p_3)^2, \tag{8}$$

which satisfy $\hat{s}+\hat{t}+\hat{u} = m_H^2$. The four tensor structures in Eq. (6) are given by

$$\begin{aligned} \mathcal{T}^{\mu\nu\rho}_{gg,1} &= -\frac{1}{2}\hat{s}p_1^\rho g^{\mu\nu} + p_2^\mu p_1^\nu p_1^\rho + \frac{\hat{s}\hat{t}p_2^\rho g^{\mu\nu}}{2\hat{u}} - \frac{\hat{t}p_2^\mu p_1^\nu p_2^\rho}{\hat{u}}, \\ \mathcal{T}^{\mu\nu\rho}_{gg,2} &= \frac{1}{2}\hat{t}p_1^\nu g^{\mu\rho} + p_3^\mu p_1^\nu p_1^\rho + \frac{\hat{s}\hat{t}p_3^\nu g^{\mu\rho}}{2\hat{u}} + \frac{\hat{s}p_3^\mu p_3^\nu p_1^\rho}{\hat{u}}, \\ \mathcal{T}^{\mu\nu\rho}_{gg,3} &= \frac{1}{2}\hat{u}p_2^\mu g^{\nu\rho} + p_2^\mu p_3^\nu p_2^\rho + \frac{\hat{s}p_3^\mu p_3^\nu p_2^\rho}{\hat{t}} + \frac{\hat{s}\hat{u}p_3^\mu g^{\nu\rho}}{2\hat{t}}, \\ \mathcal{T}^{\mu\nu\rho}_{gg,4} &= -\frac{1}{2}\hat{s}p_3^\mu g^{\nu\rho} + \frac{1}{2}\hat{s}p_3^\nu g^{\mu\rho} - \frac{1}{2}\hat{t}p_2^\mu g^{\nu\rho} + \frac{1}{2}\hat{t}p_2^\rho g^{\mu\nu} \\ &\quad + \frac{1}{2}\hat{u}p_1^\nu g^{\mu\rho} - \frac{1}{2}\hat{u}p_1^\rho g^{\mu\nu} - p_2^\mu p_3^\nu p_1^\rho + p_3^\mu p_1^\nu p_2^\rho. \end{aligned} \tag{9}$$

And the two tensor structures in Eq. (7) are given by

$$\begin{aligned} \mathcal{T}^{\rho}_{q\bar{q},1} &= \frac{\hat{t}}{2}\bar{v}(p_2)\gamma^\rho u(p_1) + \bar{v}(p_2)\not{p}_3 u(p_1)p_1^\rho, \\ \mathcal{T}^{\rho}_{q\bar{q},2} &= \frac{\hat{u}}{2}\bar{v}(p_2)\gamma^\rho u(p_1) + \bar{v}(p_2)\not{p}_3 u(p_1)p_2^\rho. \end{aligned} \tag{10}$$

Note that these tensor structures are organized such that the form factors $A_{gg,i}$ and $A_{q\bar{q},i}$ are gauge invariant. To calculate the form factors, we generate the relevant Feynman diagrams using FeynArts [23]. The resulting amplitudes are further manipulated with FeynCalc [24–26]. Finally, two sets of projection operators constructed from Eqs. (9) and (10) are used to extract $A_{gg,i}$ and $A_{q\bar{q},i}$ from the amplitudes $\mathcal{M}^{\mu\nu\rho}_{abc}$ and $\mathcal{M}^{\rho}_{abc}$ respectively, which can be found in Ref. [27]. The form factors can be perturbatively expanded according to

$$A_{gg(q\bar{q}),i} = \frac{\alpha_s}{4\pi}\left[A^{(0)}_{gg(q\bar{q}),i} + \frac{G_F}{2\sqrt{2}\pi^2}A^{(1)}_{gg(q\bar{q}),i} + \mathcal{O}(G_F^2)\right], \tag{11}$$

where $A^{(0)}_{gg(q\bar{q}),i}$ are the one-loop contributions which are known exactly and $A^{(1)}_{gg(q\bar{q}),i}$ are the two-loop contributions which involve the two-loop Feynman integrals with four independent scales $\hat{s}$, $\hat{t}$, m_t^2, and m_H^2. For $A^{(1)}_{gg(q\bar{q}),i}$, we only calculate the contributions coming from the two-loop Feynman diagrams with a λ_{HHH} vertex, denoted by $A^{(1),\rm bare}_{gg(q\bar{q}),i}$. A straightforward calculation of these two-loop Feynman diagrams is very challenging for two reasons. First, it is very difficult to perform the integration-by-parts (IBP) reduction for the nonplanar integral family. Second, the analytic results of the relevant master integrals are by far unknown. To tackle these challenging calculations, we apply the large top-quark mass expansion to $A^{(1),\rm bare}_{gg(q\bar{q}),i}$. Based on the method of expansion by regions, the integration domain of the loop momenta (l_1, l_2) is divided into four regions: hard-hard, hard-soft, soft-hard, and soft-soft. According to the definition of l_1 and l_2 shown in

Fig. 1, only hard-hard and hard-soft regions contribute. Combining the contribution from these two regions, we obtain the final results of the Feynman integrals in the limit $m_t^2 \gg \hat{s}, |\hat{t}|, m_H^2$.

In our work, $A^{(1),\text{bare}}_{gg(q\bar{q}),i}$ are expanded up to $\mathcal{O}[1/(m_t^2)^6]$ (N^{6}LP). The most time-consuming part is the IBP reduction of a huge number of Feynman integrals after expansion by regions. Up to N^{6}LP, there are about 10 million Feynman integrals before IBP reduction. In the large top-quark mass limit, the structures of the form factors $A^{(1),\text{bare}}_{gg(q\bar{q}),i}$ are very simple. Schematically, we present the $\mathcal{O}[1/(m_t^2)^0]$ (LP) contributions to $A^{(1),\text{bare}}_{gg,i}$ as

$$\vec{A}^{(1),\text{bare}}_{gg} = \frac{m_H^2}{12}(-12L_m + 4\sqrt{3}\pi - 23) \times \left(\frac{1}{\hat{t}}, \frac{1}{\hat{s}}, -\frac{1}{\hat{s}}, \frac{1}{\hat{s}} + \frac{1}{\hat{t}} + \frac{1}{\hat{u}}\right), \tag{12}$$

where $L_m = \ln(m_t^2/m_H^2)$, the $\sqrt{3}\pi$ terms come from the hard-soft region of the two-loop integrals, and $A^{(1),\text{bare}}_{gg,i}$ is the ith element of $\vec{A}^{(1),\text{bare}}_{gg}$. Note that there are no UV and IR divergences in the form factors.

To investigate the validity of large top-quark mass expansion, we also expand the one-loop amplitudes up to $\mathcal{O}[1/(m_t^2)^{12}]$, which is essential for constructing the [6/6] Padé approximation used in the next section. We will compare the approximate results with the exact results at LO in the next section. For the exact results at LO, we evaluate the one-loop scalar Feynman integrals using program libraries LOOPTOOLS [28] and QCDLOOP [29]. We have checked that our LO integrated cross sections are in good agreement with those of MadGraph5_AMC@NLO [30] where the relative errors from Monte Carlo integration are about 0.5%.

At NLO, the form factors $A^{(1),\text{bare}}_{gg(q\bar{q}),i}$ have been given up to N^{3}LP in Ref. [16]. It should be noted that the conventions for the form factors are different between Ref. [16] and our work, because of the different choices of tensor structures and normalization factors. After the necessary transformation to arrive at their convention, we find that our results agree with those given in Ref. [16]. For reference, we show the analytic results of $A^{(1),\text{bare}}_{gg(q\bar{q}),i}$ up to N^{4}LP in the Appendix and give $A^{(1),\text{bare}}_{gg(q\bar{q}),i}$ up to N^{6}LP in an electronic file attached to the arXiv submission, together with $A^{(0)}_{gg(q\bar{q}),i}$ up to N^{12}LP used in our work.

Note that the large top-quark mass approximation is formally valid only below the $2m_t$ threshold. To extend our predictions beyond that region, we adopt the Padé approximation [18–22]. Following Ref. [18], we apply Padé approximation to the series expansion in terms of the variable

$$w \equiv \frac{1 - \sqrt{1 - s'/(4m_t^2)}}{1 + \sqrt{1 - s'/(4m_t^2)}}, \tag{13}$$

instead of the variable $1/m_t^2$. Note that $s' = \hat{s}$ for the gg channel and $q\bar{q}$ channel and $s' = \hat{t}$ for the qg channel. The form factors can therefore be expanded in w as

$$A_i^{(j)}(w) = \sum_{n=0}^{\infty} a_{i,n}^{(j)} w^n. \tag{14}$$

We insert Eq. (14) into Eq. (5) and calculate the interference with the unexpanded one-loop amplitudes, which is given by

$$\left[\mathcal{M}^{*(0)}\mathcal{M}^{(j)}\right](w) = \sum_{n=0}^{\infty} b_n^{(j)} w^n. \tag{15}$$

Note that $b_n^{(j)}$ receive contributions not only from $a_{i,n}^{(j)}$ for various i but also from $\mathcal{M}^{*(0)}$, which is not expanded in w. The resulting $[m/n]$ Padé approximation for the squared amplitudes takes the form

$$\left[\mathcal{M}^{*(0)}\mathcal{M}^{(j)}\right]_{[m/n]} = \frac{c_0^{(j)} + c_1^{(j)} w + \cdots + c_m^{(j)} w^m}{1 + d_1^{(j)} w + \cdots + d_n^{(j)} w^n}, \tag{16}$$

where the coefficients $c_i^{(j)}$ and $d_i^{(j)}$ can be uniquely determined by the first $m + n + 1$ coefficients $b_i^{(j)}$. $[\mathcal{M}^{*(0)}\mathcal{M}^{(j)}]_{[m/n]}$ can now be use to calculate the Padé approximated cross sections. With the above knowledge, we can give our numerical predictions for the C_1 parameter defined in Eq. (4).

III. NUMERICAL RESULTS

In this section, we present our numerical predictions for the total cross section, the m_{jh} distribution, and the p_T distribution, where $m_{jh} = \sqrt{(p_3 + p_4)^2} = \sqrt{\hat{s}}$ is the invariant mass of the Higgs boson and the final state jet, and p_T is the transverse momentum of the Higgs boson. We choose the input parameters as $m_t = 172.5$ GeV, $m_H = 125.25$ GeV, and $G_F = 1.1663787 \times 10^{-5}$ GeV^{-2} [31]. The hadronic center-of-mass energy is chosen as $\sqrt{s} = 13.6$ TeV. We use `CT18NNLO_as_0118`[32] for the evaluation of both LO and NLO cross sections through the LHAPDF interface [33]. For the strong coupling constant, we use the value provided by `CT18NNLO_as_0118`: $\alpha_s(m_Z) = 0.118$. The default factorization scale μ_f and renormalization scale μ_r are chosen as $\mu_f = \mu_r = (\sqrt{p_T^2 + m_H^2} + p_T)/2$. Last but not least, we choose the cut $p_T \geq 20$ GeV to get finite predictions for the total cross section as well as the m_{jh} distribution.

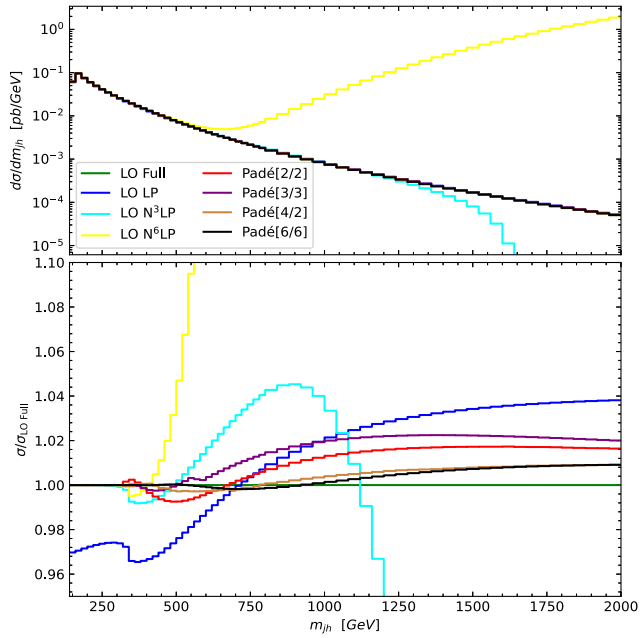

FIG. 2. The LO differential cross sections of $pp \to H + j$ with respect to the invariant mass m_{jh} of the Higgs boson and the jet. The lower plot shows the ratios to the LO exact values.

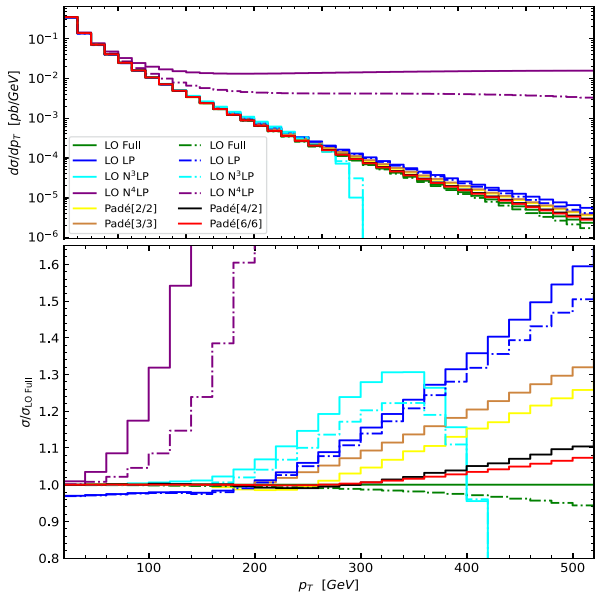

FIG. 3. The LO differential cross sections of $pp \to H + j$ with respect to the transverse momentum p_T of the Higgs boson. The solid lines show the distributions without the $\hat{s}$ cut, while the dashed lines show the distributions with the $\hat{s}$ cut. The lower plot shows the ratios to the LO exact values without the $\hat{s}$ cut.

We first present LO results. We show in Fig. 2 the LO differential cross sections for m_{jh}. To see the performance of large top-quark mass expansion clearly, we present the exact distribution and the distribution up to $\mathcal{O}[1/(m_t^2)^n]$ (N^{n}LP). The upper plot employs a logarithmic scale for the vertical axis to give the distributions in the broad range 140 GeV $\leq m_{jh} \leq$ 2000 GeV. The lower plot shows the ratios to the exact values of the LO differential cross section. As we expected, the distributions in the region $m_{jh} \leq 2m_t$ show excellent convergence of the large top-quark mass expansion. The relative errors of N^{3}LP are already smaller than 0.3%. However, the distributions at N^{3}LP and N^{6}LP blow up beyond $2m_t$ threshold, which are clear in the lower plot of Fig. 2. To get reliable estimations in the $m_{jh} \geq 2m_t$ region, we apply the Padé approximation to the series expansion in w. Using the expansion up to N^{12}LP, we can construct $[m/n]$ Padé approximation with $m + n \leq 12$. We show the distributions with $[2/2]$, $[3/3]$, $[4/2]$, and $[6/6]$ Padé approximation in Fig. 2. We have also calculated the distributions with $[2/3]$, $[3/2]$, $[2/4]$, and $[3/4]$ Padé approximations and find that they lie within the area between $[3/3]$ and $[4/2]$ in almost the whole phase-space region. We therefore do not show these curves in Fig. 2. We can find that the relative errors of $[4/2]$ are smaller than 1% for $m_{jh} \leq 2000$ GeV.

We now turn to the p_T distribution at the LO. We have again attempted different combinations of m and n. We show only the representative curves of $[2/2]$, $[3/3]$, $[4/2]$, and $[6/6]$ Padé approximations in Fig. 3. In the small p_T region, the performance of large top-quark mass expansion with the Padé approximation is very similar to that in m_{jh} distribution. All the results with Padé approximations may serve as reliable estimations of the exact results. However, in the large p_T region, the predictions with Padé approximation show as much as 10% relative errors, which is significantly different from the case of the m_{jh} distribution. Specifically, the relative errors of $[4/2]$ Padé approximation reach 1% in the region $p_T \in [340, 360]$ GeV and reach 10% in the region $p_T \in [500, 520]$ GeV. It is possible to further improve the Padé approximation by including higher power corrections in w. Indeed, the $[6/6]$ Padé approximation gives better predictions than those of the $[4/2]$ Padé approximation in the large p_T region.

The Padé approximation works better in the large m_{jh} region than in the large p_T region, which can be partly attributed to the following fact. The distribution in the large p_T region only receives the contributions from the large m_{jh} region, while the one in the large m_{jh} region receives dominant contributions from the small p_T region. Because of this, the validity range of the approximations for the p_T distribution is much smaller than the naive guess $p_T < m_t$, which can be seen from the lower plot of Fig. 3. To show the significant influence from the large $\hat{s}$ region to the p_T distribution, we further impose an $\hat{s}$ cut $\sqrt{\hat{s}} \leq 2000$ GeV in the calculations. The results are shown in Fig. 3 as dashed lines. We find that this $\hat{s}$ cut can improve the convergence to some extent, which can be clearly seen from the N^{4}LP curves with/without the $\hat{s}$ cut. Because the dominant contributions to the total cross section come from the small m_{jh} region, the $\hat{s}$ cut should not give significant

TABLE I. The LO integrated cross sections (in pb) for $p_T \geq 20$ GeV. σ_{exact} is the exact result. $\sigma_{\text{N}^n\text{LP}}$ are the results with the large top-quark mass expansion up to $\mathcal{O}[1/(m_t^2)^n]$. $\sigma_{[m/n]}$ are the results using $[m/n]$ Padé approximations. The error of each number from Monte Carlo integration is given in parentheses.

$\hat{s}$ cut	σ_{exact}	σ_{LP}	$\sigma_{\text{N}^3\text{LP}}$	$\sigma_{[4/2]}$	$\sigma_{[6/6]}$
No	13.651(5)	13.304(5)	13.089(5)	13.647(3)	13.652(5)
Yes	13.628(1)	13.280(1)	13.563(1)	13.624(3)	13.628(1)

influence on the integrated cross sections. We show the LO integrated cross sections for $p_T \geq 20$ GeV with and without the $\hat{s}$ cut in Table I. We find that the contribution from the region above the $\hat{s}$ cut is only about 0.2%. As is expected, the $\hat{s}$ cut makes the approximate results, e.g., N^{3}LP, more compatible with the exact one. The $[4/2]$ and $[6/6]$ Padé approximations show precise estimations of the exact result.

We now move to the main results of this paper, i.e., the NLO corrections proportional to λ_{HHH}. As is clear from Eq. (2), the information about the NLO corrections is fully encoded in the C_1 parameter (note that δZ_H is kinematics independent). Therefore, in the following, we give our predictions for the C_1 parameter using Eq. (4). In Fig. 4, we give the C_1 parameter in its differential form with respect to m_{jh}. We find that the N^{6}LP and Padé approximations give consistent results in the $m_{jh} \leq 2m_t$ region, where the large top-quark mass expansion is valid. These are similar to the cases at the LO. However, there are two significant differences between C_1 and the LO differential cross sections. One is that the LP contribution is dominant at LO, while the LP only accounts for about half of C_1. The other is that the trends of N^{n}LP (e.g., $n = 3$ and $n = 6$) curves for C_1 are opposite to the corresponding LO ones when $m_{jh} > 2m_t$. Because of these two differences, the approximation scheme to the full theory (FT$_{\text{approx}}$) [34], which is a remarkably reliable method for NLO QCD corrections to $pp \to H + j$ [12,13], is not applicable in our case. We use the $[4/2]$ Padé approximation as our best

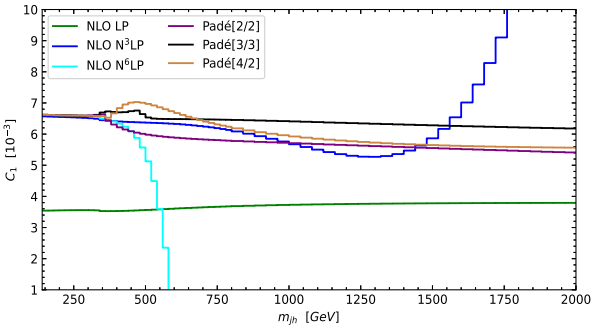

FIG. 4. The C_1 parameters with respect to the invariant mass m_{jh} of the Higgs boson and the jet.

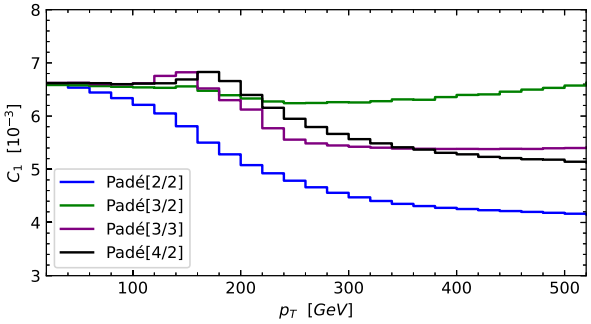

FIG. 5. The C_1 parameters with respect to the transverse momentum p_T of the Higgs boson. The $\hat{s}$ cut is not applied.

predictions at NLO in m_{jh} distribution. We note that the dependence of the differential C_1 parameter on the invariant mass m_{jh} is very weak, with its values being around 0.6% across the whole phase-space region. According to the behavior of the $[4/2]$ Padé approximation at LO, we believe that the predictions at NLO are quite accurate in the convergent region and are reliable in the high-energy region with their relative errors being at the level of a few percent. The small humps near $2m_t$ threshold region are expected to come from the large top-quark mass expansion with Padé approximation and will be flattened when higher-order Padé approximations are considered. Similar behaviors are observed at the LO.

We then show in Fig. 5 the differential C_1 parameter with respect to p_T. We emphasize that in the large p_T region, results from Padé approximations can only be used to get a rough estimation of the exact result, with relative errors at the level of 10%. Based on the analyses at LO, we believe that the $[4/2]$ Padé approximation is a reasonable approximation at NLO as well. It is consistent with the $[3/2]$ and $[3/3]$ approximations in the small p_T region. The expansion at the NLO shows a slower convergence than that at the LO. In the small p_T region, the $[2/2]$ approximation has large deviations from other curves and is not reliable. In the large p_T region, the predictions of the $[4/2]$ Padé approximation are consistent with those of the $[3/2]$ and $[3/3]$ approximations within the relative errors estimated according to the LO results. Across the whole range, the values of C_1 is around 0.6%, similar to the case in the m_{jh} distribution.

TABLE II. Values of C_1 for total corrections. $C_1^{\text{N}^n\text{LP}}$ corresponds to large top-quark mass expansion up to $\mathcal{O}[1/(m_t^2)^n]$. $C_1^{[m/n]}$ corresponds to the prediction of the $[m/n]$ Padé approximation. The relative error of each number from Monte Carlo integration is less than 0.5%.

$\hat{s}$ cut	C_1^{LP}	$C_1^{\text{N}^3\text{LP}}$	$C_1^{[3/3]}$	$C_1^{[4/2]}$
No	0.0036	0.0067	0.0066	0.0066
Yes	0.0036	0.0065	0.0066	0.0066

These behaviors show that C_1 has only a very mild kinematics-dependence.

Finally, we give the C_1 parameter for total corrections which is defined as the ratio between NLO corrections and LO total cross section in Table II. Our best prediction at NLO gives $C_1 = 0.66\%$.

IV. CONCLUSION

In this work, we calculate the corrections proportional to the Higgs trilinear self-coupling λ_{HHH} for Higgs boson plus one jet production at the LHC. We perform an asymptotic expansion in the large top-quark mass limit with the method of expansion by regions. The prediction is then extended to high-energy regions by applying the Padé approximation. We use the $[4/2]$ Padé approximation as our best prediction at the NLO. We find the values of C_1 at the differential level have a mild dependence on the kinematic variables m_{jh} and p_T and are mostly in the range 0.5%–0.7%. As for the C_1 parameter for total corrections, the value is 0.66%.

The values of C_1 is small, which is common for λ_{HHH}-related corrections. Similar effects have been found in $gg \to H$, VBF, and VH production channels and also in various decay channels of the Higgs boson [6,7]. The expected experimental precisions for these production channels are also similar at the high-luminosity large hadron collider [35,36]. On the other hand, these channels are not expected to be used alone but should be combined altogether with double-Higgs production channels, as is done in Ref. [3]. Hence, our results provide an additional channel to set extra constraints on λ_{HHH} from the experimental data.

The high-energy behavior of the approximation at NLO can be further improved by including higher-order Padé approximation, which needs higher power expansion in the large top-quark mass limit. The calculation is straightforward, while the IBP reduction, which is the most time-consuming part as mentioned before, would take much more time. For example, to calculate N^{7}LP corrections at NLO, we still need to perform IBP reduction on about 12 million Feynman integrals. This is much more difficult than N^{6}LP and is expected to take several months. Note that constructing the $[6/6]$ Padé approximation requires the two-loop Feynman integrals to be expanded up to N^{12}LP. However, the $[6/6]$ Padé approximation is still not accurate enough especially in the large p_T region, as observed at the LO. Therefore, in the large p_T region, it is necessary to employ a more efficient method, for example, the high-energy expansion of Refs. [37–40] or the small mass expansion of Refs. [41–43]. The latter method is applicable in the whole phase-space region of interest, as was shown in the cases of $gg \to H + H$ and $gg \to H + Z$ processes. Alternatively, one may evaluate the two-loop integrals numerically using the auxiliary mass flow method [44–48]. These are left for future investigations.

ACKNOWLEDGMENTS

The authors would like to thank Yanping Huang for useful discussion. This work was supported in part by the National Natural Science Foundation of China under Grants No. 11975030, No. 12147103, and No. 11925506 and the Fundamental Research Funds for the Central Universities. This work of J. Gao is sponsored by the National Natural Science Foundation of China under Grants No. 12275173 and No. 11835005. The research of G. Wang was supported in part by the International Postdoctoral Exchange Fellowship Program from China Postdoctoral Council under Grant No. PC2021066. The work of X. Shen is supported in part by the Helmholtz-OCPC Postdoctoral Exchange Program under Grant No. ZD2022004.

APPENDIX: THE ANALYTIC RESULTS FOR THE FORM FACTORS

In this Appendix, we provide the analytical results for $A^{(1),\text{bare}}_{gg(q\bar{q}),i}$ up to N^{4}LP. First, we present the form factors of the gluon fusion channel. For the $A^{(1),\text{bare}}_{gg,i,\text{NLP}}$, we have

$$\begin{aligned} A^{(1),\text{bare}}_{gg,1,\text{NLP}} &= -\frac{m_H^4}{m_t^2 \hat{t}} a_1, \\ A^{(1),\text{bare}}_{gg,4,\text{NLP}} &= \frac{m_H^2}{m_t^2 \hat{s}} \left\{ \frac{m_H^2}{\hat{t}\,\hat{u}} [\hat{t}^2 + \hat{u}^2 - m_H^2(\hat{t} + \hat{u})] a_1 \right. \\ &\quad \left. + m_H^2 a_2 - (\hat{t} + \hat{u}) a_3 \right\}, \end{aligned} \tag{A1}$$

where

$$\begin{aligned} a_1 &= \frac{7L_m}{10} - \frac{7\pi}{20\sqrt{3}} + \frac{259}{240}, \\ a_2 &= \frac{31L_m}{40} - \frac{17\pi}{40\sqrt{3}} + \frac{1487}{1200}, \\ a_3 &= \frac{3L_m}{40} - \frac{\sqrt{3}\pi}{40} + \frac{4}{25}. \end{aligned} \tag{A2}$$

For the $A^{(1),\text{bare}}_{gg,i,\text{N}^2\text{LP}}$, we have

$$\begin{aligned} A^{(1),\text{bare}}_{gg,1,\text{N}^2\text{LP}} &= -\frac{m_H^2}{m_t^4 \hat{t}} [m_H^4 b_1 + \hat{t}\,\hat{u} b_2], \\ A^{(1),\text{bare}}_{gg,4,\text{N}^2\text{LP}} &= \frac{m_H^4}{m_t^4 \hat{s}} \left\{ \frac{m_H^2}{\hat{t}\,\hat{u}} [\hat{t}^2 + \hat{u}^2 - m_H^2(\hat{t} + \hat{u})] b_1 \right. \\ &\quad \left. + m_H^2 b_3 - (\hat{t} + \hat{u}) b_4 \right\}, \end{aligned} \tag{A3}$$

where

$$b_1 = \frac{349L_m}{1008} - \frac{23\pi}{240\sqrt{3}} + \frac{464419}{1058400},$$
$$b_2 = \frac{L_m}{140} - \frac{\pi}{280\sqrt{3}} + \frac{37}{50400},$$
$$b_3 = \frac{1853L_m}{5040} - \frac{179\pi}{1680\sqrt{3}} + \frac{1092101}{2116800},$$
$$b_4 = \frac{3L_m}{140} - \frac{\sqrt{3}\pi}{280} + \frac{54421}{705600}. \tag{A4}$$

For the $A^{(1),\text{bare}}_{gg,i,\text{N}^3\text{LP}}$, we have

$$A^{(1),\text{bare}}_{gg,1,\text{N}^3\text{LP}} = -\frac{m_H^2}{m_t^6\hat{t}}[m_H^6 c_1 + m_H^2\hat{t}\hat{u}c_2 - \hat{t}\hat{u}(\hat{t}+\hat{u})c_3],$$
$$A^{(1),\text{bare}}_{gg,4,\text{N}^3\text{LP}} = \frac{m_H^2}{m_t^6\hat{s}}\left\{\frac{m_H^6}{\hat{t}\hat{u}}[\hat{t}^2+\hat{u}^2 - m_H^2(\hat{t}+\hat{u})]c_1 + m_H^6 c_4 + m_H^4(\hat{t}+\hat{u})c_5 + [\hat{s}(2\hat{t}^2+3\hat{t}\hat{u}+2\hat{u}^2) + (\hat{t}+\hat{u})^3]c_6\right\}, \tag{A5}$$

where

$$c_1 = \frac{1741L_m}{10800} - \frac{13\pi}{525\sqrt{3}} + \frac{31795373}{190512000},$$
$$c_2 = \frac{1717L_m}{126000} - \frac{533\pi}{126000\sqrt{3}} + \frac{254311}{79380000},$$
$$c_3 = \frac{113L_m}{42000} - \frac{521\pi}{126000\sqrt{3}} + \frac{188969}{45360000},$$
$$c_4 = \frac{18541L_m}{126000} - \frac{407\pi}{18000\sqrt{3}} + \frac{9462017}{52920000},$$
$$c_5 = \frac{233L_m}{25200} + \frac{\pi}{360\sqrt{3}} - \frac{142763}{9072000},$$
$$c_6 = \frac{1817L_m}{378000} - \frac{23\sqrt{3}\pi}{14000} + \frac{1825337}{476280000}. \tag{A6}$$

For the $A^{(1),\text{bare}}_{gg,i,\text{N}^4\text{LP}}$, we have

$$A^{(1),\text{bare}}_{gg,1,\text{N}^4\text{LP}} = \frac{m_H^2\hat{u}}{m_t^8}\left[\frac{m_H^8}{\hat{t}\hat{u}}d_1 - m_H^2(\hat{t}+\hat{u})d_2 + m_H^4 d_3 + (\hat{t}^2+\hat{u}^2)d_4 + \hat{t}\hat{u}d_5\right],$$
$$A^{(1),\text{bare}}_{gg,4,\text{N}^4\text{LP}} = \frac{m_H^2}{m_t^8\hat{s}}\left\{\frac{m_H^8}{\hat{t}\hat{u}}[\hat{t}^2+\hat{u}^2 - m_H^2(\hat{t}+\hat{u})]d_1 + m_H^4\hat{t}\hat{u}d_6 + m_H^4(\hat{t}^2+\hat{u}^2)d_7 + m_H^8 d_8 - (\hat{t}+\hat{u})[m_H^2(\hat{t}^2+\hat{u}^2)d_9 + m_H^2\hat{t}\hat{u}d_{10} - \hat{t}\hat{u}(\hat{t}+\hat{u})d_{11} - m_H^6 d_{12}]\right\}, \tag{A7}$$

where

$$d_1 = \frac{10817L_m}{138600} - \frac{1789\pi}{277200\sqrt{3}} + \frac{40370773}{614718720},$$
$$d_2 = \frac{55249L_m}{8316000} - \frac{1067\pi}{252000\sqrt{3}} + \frac{106841597}{25613280000},$$
$$d_3 = \frac{35473L_m}{2079000} - \frac{4573\pi}{1386000\sqrt{3}} + \frac{240175891}{57629880000},$$
$$d_4 = \frac{227L_m}{1663200} - \frac{19\pi}{184800\sqrt{3}} + \frac{272233}{23051952000},$$
$$d_5 = \frac{2L_m}{17325} + \frac{\pi}{11550\sqrt{3}} - \frac{9083}{34303500},$$
$$d_6 = \frac{82219L_m}{2772000} - \frac{13007\pi}{924000\sqrt{3}} + \frac{86605417}{5488560000},$$
$$d_7 = \frac{53971L_m}{2772000} - \frac{26539\pi}{2772000\sqrt{3}} + \frac{367056113}{32931360000},$$
$$d_8 = \frac{993907L_m}{16632000} - \frac{29401\pi}{5544000\sqrt{3}} + \frac{2544943799}{41912640000},$$
$$d_9 = \frac{53971L_m}{5544000} - \frac{26539\pi}{5544000\sqrt{3}} + \frac{367056113}{65862720000},$$
$$d_{10} = \frac{59021L_m}{5544000} - \frac{23389\pi}{5544000\sqrt{3}} + \frac{243249443}{65862720000},$$
$$d_{11} = \frac{101L_m}{221760} + \frac{\pi}{3520\sqrt{3}} - \frac{4126889}{4390848000},$$
$$d_{12} = \frac{7111L_m}{831600} + \frac{\pi}{275\sqrt{3}} - \frac{1058129}{1707552000}. \tag{A8}$$

Because of the crossing symmetry, we have

$$A^{(1),\text{bare}}_{gg,2,\text{N}^j\text{LP}} = A^{(1),\text{bare}}_{gg,1,\text{N}^j\text{LP}}(\hat{s}\leftrightarrow\hat{t}),$$
$$A^{(1),\text{bare}}_{gg,3,\text{N}^j\text{LP}} = -A^{(1),\text{bare}}_{gg,2,\text{N}^j\text{LP}}(\hat{t}\leftrightarrow\hat{u}). \tag{A9}$$

Then, we give the form factors of the quark-antiquark annihilation channel. For the $A^{(1),\text{bare}}_{q\bar{q},i,\text{LP}}$, we have

$$A^{(1),\text{bare}}_{q\bar{q},1,\text{LP}} = \frac{m_H^2}{\hat{s}}\left(\frac{L_m}{2} - \frac{\pi}{2\sqrt{3}} + \frac{23}{24}\right). \tag{A10}$$

For the $A^{(1),\text{bare}}_{q\bar{q},1,\text{NLP}}$, we have

$$A^{(1),\text{bare}}_{q\bar{q},1,\text{NLP}} = \frac{m_H^2}{\hat{s}}(m_H^2 a_1^q + \hat{s}a_2^q), \tag{A11}$$

where

$$a_1^q = \frac{7L_m}{20} - \frac{7\pi}{40\sqrt{3}} + \frac{259}{480},$$
$$a_2^q = \frac{11L_m}{90} - \frac{11\pi}{120\sqrt{3}} + \frac{863}{7200}. \tag{A12}$$

For the $A^{(1),\text{bare}}_{q\bar{q},1,\text{N}^2\text{LP}}$, we have

$$A^{(1),\text{bare}}_{q\bar{q},1,\text{N}^2\text{LP}} = \frac{m_H^2}{\hat{s}}(m_H^2\hat{s}b_1^q + m_H^4 b_2^q + \hat{s}^2 b_3^q), \tag{A13}$$

where

$$b_1^q = \frac{1271L_m}{10080} - \frac{167\pi}{3360\sqrt{3}} + \frac{266837}{2116800},$$
$$b_2^q = \frac{349L_m}{2016} - \frac{23\pi}{480\sqrt{3}} + \frac{464419}{2116800},$$
$$b_3^q = \frac{11L_m}{420} - \frac{11\pi}{840\sqrt{3}} + \frac{17}{5040}. \tag{A14}$$

For the $A^{(1),\text{bare}}_{q\bar{q},1,\text{N}^3\text{LP}}$, we have

$$A^{(1),\text{bare}}_{q\bar{q},1,\text{N}^3\text{LP}} = \frac{m_H^2}{\hat{s}}(m_H^6 c_1^q + m_H^4 \hat{s} c_2^q + m_H^2 \hat{s}^2 c_3^q + \hat{s}^3 c_4^q), \tag{A15}$$

where

$$c_1^q = \frac{1741L_m}{21600} - \frac{13\pi}{1050\sqrt{3}} + \frac{31795373}{381024000},$$
$$c_2^q = \frac{125863L_m}{1512000} - \frac{9109\pi}{504000\sqrt{3}} + \frac{1480511}{19440000},$$
$$c_3^q = \frac{19483L_m}{504000} - \frac{731\pi}{72000\sqrt{3}} + \frac{1296991}{79380000},$$
$$c_4^q = \frac{301L_m}{54000} - \frac{\sqrt{3}\pi}{1750} - \frac{5466617}{1905120000}. \tag{A16}$$

For the $A^{(1),\text{bare}}_{q\bar{q},1,\text{N}^4\text{LP}}$, we have

$$A^{(1),\text{bare}}_{q\bar{q},1,\text{N}^4\text{LP}} = \frac{m_H^2}{\hat{s}}(m_H^8 d_1^q + m_H^6 \hat{s} d_2^q + m_H^4 \hat{s}^2 d_3^q + m_H^2 \hat{s}^3 d_4^q + \hat{s}^4 d_5^q), \tag{A17}$$

where

$$d_1^q = \frac{10817L_m}{277200} - \frac{1789\pi}{554400\sqrt{3}} + \frac{40370773}{1229437440},$$
$$d_2^q = \frac{28151L_m}{594000} - \frac{4999\pi}{924000\sqrt{3}} + \frac{17411038151}{461039040000},$$
$$d_3^q = \frac{52319L_m}{1512000} - \frac{1051\sqrt{3}\pi}{616000} + \frac{8206234093}{461039040000},$$
$$d_4^q = \frac{184463L_m}{16632000} - \frac{2813\pi}{1848000\sqrt{3}} - \frac{557260999}{461039040000},$$
$$d_5^q = \frac{997L_m}{831600} - \frac{79\pi}{277200\sqrt{3}} - \frac{29741}{28459200}. \tag{A18}$$

Because of the crossing symmetry, we have $A^{(1),\text{bare}}_{q\bar{q},2,\text{N}^j\text{LP}} = A^{(1),\text{bare}}_{q\bar{q},1,\text{N}^j\text{LP}}$.

[1] G. Aad *et al.* (ATLAS Collaboration), Phys. Lett. B **716**, 1 (2012).
[2] S. Chatrchyan *et al.* (CMS Collaboration), Phys. Lett. B **716**, 30 (2012).
[3] ATLAS Collaboration, arXiv:2211.01216.
[4] E. W. N. Glover and J. J. van der Bij, Nucl. Phys. **B309**, 282 (1988).
[5] T. Plehn, M. Spira, and P. M. Zerwas, Nucl. Phys. **B479**, 46 (1996); **B531**, 655(E) (1998).
[6] G. Degrassi, P. P. Giardino, F. Maltoni, and D. Pagani, J. High Energy Phys. 12 (2016) 080.
[7] F. Maltoni, D. Pagani, A. Shivaji, and X. Zhao, Eur. Phys. J. C **77**, 887 (2017).
[8] M. Becchetti, R. Bonciani, V. Casconi, V. Del Duca, and F. Moriello, J. High Energy Phys. 12 (2018) 019.
[9] M. Bonetti, E. Panzer, V. A. Smirnov, and L. Tancredi, J. High Energy Phys. 11 (2020) 045.
[10] M. Becchetti, F. Moriello, and A. Schweitzer, J. High Energy Phys. 04 (2022) 139.
[11] M. Bonetti, E. Panzer, and L. Tancredi, J. High Energy Phys. 06 (2022) 115.
[12] X. Chen, J. Cruz-Martinez, T. Gehrmann, E. W. N. Glover, and M. Jaquier, J. High Energy Phys. 10 (2016) 066.
[13] X. Chen, A. Huss, S. P. Jones, M. Kerner, J. N. Lang, J. M. Lindert, and H. Zhang, J. High Energy Phys. 03 (2022) 096.
[14] J. Grigo, J. Hoff, and M. Steinhauser, Nucl. Phys. **B900**, 412 (2015).
[15] M. Grazzini, G. Heinrich, S. Jones, S. Kallweit, M. Kerner, J. M. Lindert, and J. Mazzitelli, J. High Energy Phys. 05 (2018) 059.
[16] M. Gorbahn and U. Haisch, J. High Energy Phys. 04 (2019) 062.
[17] B. Di Micco *et al.*, Rev. Phys. **5**, 100045 (2020).
[18] J. Fleischer and O. V. Tarasov, Z. Phys. C **64**, 413 (1994).
[19] J. Fleischer, V. A. Smirnov, and O. V. Tarasov, Z. Phys. C **74**, 379 (1997).
[20] R. V. Harlander, in *Proceedings of the 5th International Symposium on Radiative Corrections: Applications of Quantum Field Theory to Phenomenology* (2001), arXiv: hep-ph/0102266.
[21] J. M. Campbell, R. K. Ellis, M. Czakon, and S. Kirchner, J. High Energy Phys. 08 (2016) 011.
[22] A. Hasselhuhn, T. Luthe, and M. Steinhauser, J. High Energy Phys. 01 (2017) 073.
[23] T. Hahn, Comput. Phys. Commun. **140**, 418 (2001).
[24] R. Mertig, M. Bohm, and A. Denner, Comput. Phys. Commun. **64**, 345 (1991).
[25] V. Shtabovenko, R. Mertig, and F. Orellana, Comput. Phys. Commun. **207**, 432 (2016).
[26] V. Shtabovenko, R. Mertig, and F. Orellana, Comput. Phys. Commun. **256**, 107478 (2020),

[27] T. Gehrmann, M. Jaquier, E. W. N. Glover, and A. Koukoutsakis, J. High Energy Phys. 02 (2012) 056.
[28] T. Hahn and M. Perez-Victoria, Comput. Phys. Commun. **118**, 153 (1999).
[29] S. Carrazza, R. K. Ellis, and G. Zanderighi, Comput. Phys. Commun. **209**, 134 (2016).
[30] J. Alwall, R. Frederix, S. Frixione, V. Hirschi, F. Maltoni, O. Mattelaer, H. S. Shao, T. Stelzer, P. Torrielli, and M. Zaro, J. High Energy Phys. 07 (2014) 079.
[31] R. L. Workman *et al.* (Particle Data Group), Prog. Theor. Exp. Phys. **2022**, 083C01 (2022).
[32] T.-J. Hou *et al.*, Phys. Rev. D **103**, 014013 (2021).
[33] A. Buckley, J. Ferrando, S. Lloyd, K. Nordström, B. Page, M. Rüfenacht, M. Schönherr, and G. Watt, Eur. Phys. J. C **75**, 132 (2015).
[34] F. Maltoni, E. Vryonidou, and M. Zaro, J. High Energy Phys. 11 (2014) 079.
[35] M. Cepeda *et al.*, CERN Yellow Rep. Monogr. **7**, 221 (2019).
[36] ATLAS and CMS Collaborations, Snowmass White Paper Contribution: Physics with the Phase-2 ATLAS and CMS Detectors, Technical Report (CERN, Geneva, 2022).
[37] J. Davies, G. Mishima, M. Steinhauser, and D. Wellmann, J. High Energy Phys. 03 (2018) 048.
[38] J. Davies, G. Mishima, M. Steinhauser, and D. Wellmann, J. High Energy Phys. 01 (2019) 176.
[39] G. Mishima, J. High Energy Phys. 02 (2019) 080.
[40] J. Davies, G. Mishima, and M. Steinhauser, J. High Energy Phys. 03 (2021) 034.
[41] X. Xu and L. L. Yang, J. High Energy Phys. 01 (2019) 211.
[42] G. Wang, Y. Wang, X. Xu, Y. Xu, and L. L. Yang, Phys. Rev. D **104**, L051901 (2021).
[43] G. Wang, X. Xu, Y. Xu, and L. L. Yang, Phys. Lett. B **829**, 137087 (2022).
[44] X. Liu, Y.-Q. Ma, and C.-Y. Wang, Phys. Lett. B **779**, 353 (2018).
[45] X. Liu, Y.-Q. Ma, W. Tao, and P. Zhang, Chin. Phys. C **45**, 013115 (2021).
[46] X. Liu and Y.-Q. Ma, Phys. Rev. D **105**, L051503 (2022).
[47] X. Liu and Y.-Q. Ma, Comput. Phys. Commun. **283**, 108565 (2023).
[48] Z.-F. Liu and Y.-Q. Ma, Phys. Rev. Lett. **129**, 222001 (2022).